Bull Earthquake Eng (2007) 5:277–301
DOI 10.1007/s10518-007-9030-9

ORIGINAL RESEARCH PAPER

Foundation–structure systems over a rupturing normal fault: Part II. Analysis of the Kocaeli case histories

Ioannis Anastasopoulos · George Gazetas

Received: 19 April 2006 / Accepted: 8 January 2007 / Published online: 6 April 2007

Abstract Motivated by the observed (successful and unsuccessful) performance of numerous structures on top of, or immediately next to a normal fault that ruptured during the Kocaeli 1999 earthquake, this paper: (i) develops a two-step finite element methodology to study the propagation of a fault rupture through soil and its interplay with the foundation–structure system, denoted hereafter "Fault Rupture–Soil–Foundation–Structure Interaction" (FR–SFSI), (ii) provides validation of the developed methodology through successful Class "A" predictions of centrifuge model tests, and (iii) applies the centrifuge-validated methodology to study one-by-one the Kocaeli case histories of the first paper (Part I). It is shown that the presence of a structure on top of an outcropping fault may have a significant influence on the rupture path: with heavy structures founded on continuous and rigid foundations, the fault rupture diverts substantially and may avoid rupturing underneath the structure. The latter undergoes rigid body rotation, with its foundation sometimes loosing contact with the bearing soil, but in most cases retaining its structural integrity. In stark contrast, buildings on isolated footings and, perhaps surprisingly, piles exert a smaller diversion of the rupture which is thus likely to outcrop between the footings or pile caps; the latter may thus undergo devastating differential displacements. It is shown that structures in the vicinity of faults can be designed to survive significant dislocations. The "secret" of successful performance lies on the continuity, stiffness, and rigidity of the foundation.

Keywords Fault rupture · Soil–structure interaction · Centrifuge model test · Case history · Foundation · Finite elements

I. Anastasopoulos · G. Gazetas (✉)
School of civil Engineering,
National Technical University, 15780, Zografou, Athens, Greece
e-mail: gazetas@ath.forthnet.gr

I. Anastasopoulos
e-mail: ianast@ekpe.gr

1 Introduction

This is the second paper in a two-paper sequence dealing with the behaviour of foundations and structures sitting directly on, or immediately adjacent to, a rupturing normal fault. The first paper (Anastasopoulos and Gazetas, 2007) presented the strong field evidence that has motivated our research: observations of the behaviour of a number of structures "on top" of the normal fault scarp which appeared in the Kocaeli earthquake of 1999 east of Gölcük, the city with the largest concentration of structural damage and human casualties. A number of structures sustained considerable damage or collapsed, while others almost "miraculously" survived ground offsets of more than 2 m in height. The macroscopic homogeneity of soil conditions in the area of study left no doubt that among the culprits of such differences in behaviour were the type, continuity, and rigidity of the foundation.

The main goal of this second paper is to present an in-depth analysis of the whole phenomenon of fault rupture propagation from the base rock to the ground surface, and of the ensuing distress of structures founded on top of, or immediately adjacent to the outcropping fault. Verification against centrifuge model tests provides confidence on the validity and robustness of the developed FE modelling technique. More specifically, the present paper:

(i) Develops a two-step finite element (FE) methodology to study fault rupture propagation through soil and its interaction with foundation–structure systems. In the first step, representing the "free-field" part of the problem, emphasis is given on the emerging deformation of the ground surface. The second step deals with the interaction between the outcropping dislocation and the structure. This is the soil–foundation–structure interaction (SFSI) problem, triggered by the propagating fault-rupture: FR–SFSI.
(ii) Provides adequate validation of the developed FE methodology through successful Class "A" predictions (Lambe 1973) of centrifuge model tests of: (a) free-field fault rupture propagation, and (b) interaction between the outcropping fault rupture and strip footings.
(iii) Applies the centrifuge-validated FE methodology to analyse one-by-one the Kocaeli case histories of the first paper, aiming to develop further insights into the mechanics of FR–SFSI. Idealised structures resting on isolated footings, rigid-box foundations, and a piled foundation are considered, although the analysis for the latter is only a first (crude) approximation.

2 Analysis methodology

To explore the interplay between a rupturing fault and a structure two-dimensional (2D) plane-strain analyses are performed herein. However, the fault rupture is always significantly longer than the length of a structure, and the rupture rarely crosses a structure exactly perpendicularly to its axis; therefore, the plane-strain assumption invoked in our analysis is only a first practical approximation. The analysis is conducted in two steps (Fig. 1). First, fault rupture propagation through soil is analysed in the free-field, ignoring the (potential) presence of a structure (Fig. 1a). Then, knowing the exact location of rupture outcropping in the free-field, the structure is placed on top, and

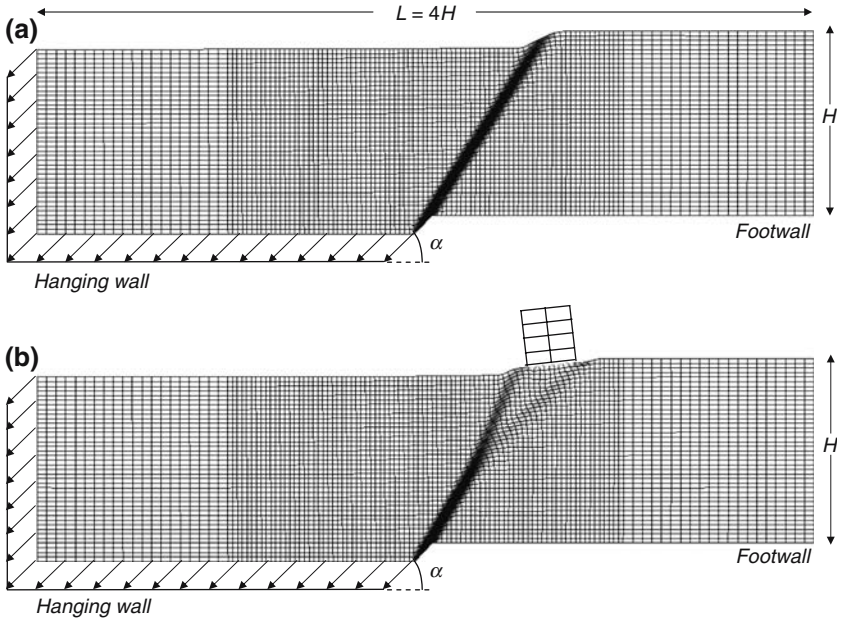

Fig. 1 Problem definition and finite element discretisation: (**a**) fault rupture propagation in the free-field, and (**b**) interplay between the outcropping fault rupture and the structure (termed Fault Rupture–Soil–Foundation–Structure Interaction, FR-SFSI)

the analysis of the soil-structure system is performed (Fig. 1b). By comparing the results of the two analyses, the effect of FR-SFSI is visualised and quantified.

2.1 Fault rupture propagation in the free-field

The problem studied in this paper along with the FE discretisation is displayed in Fig. 1a. It refers to a uniform soil deposit of thickness H at the base of which a normal fault, dipping at angle a (measured from the horizontal), ruptures and produces downward displacement, with a vertical component h. Following the recommendation of Bray (1990) and to minimise undesired boundary effects, we set the width L of the FE model equal to $4H$. The discretisation is finer in the central part of the model, with the quadrilateral elements being 1 m × 1 m (width × height). At the two edges, where limited deformation is expected, coarser meshing is used: 2 m × 1 m. The differential displacement is applied to the left part of the model (hanging-wall) in small consecutive quasi-static steps.

Soil behaviour after failure has been shown to play a major role in problems related to shear-band formation and propagation. Scott and Schoustra (1974) applying the FE method in combination with elastic–perfectly plastic constitutive soil model with Mohr–Coulomb failure criterion, produced results contradicting both reality and experiments. In contrast, Bray (1990) and Bray et al. (1994 a,b) also utilising the FE method, but with a hyperbolic non-linear elastic constitutive law achieved satisfactory agreement with small-scale tests (Bray et al., 1993). Analyses performed by Roth et al. (1981, 1982), Loukidis (1999), and Erickson et al. (2001) were also successful. They all applied the finite difference (FD) method with elastoplastic constitutive model,

Mohr–Coulomb failure criterion, and strain softening. Similar constitutive models have been successfully employed in modeling the failure of embankments and the delayed collapse of cut slopes (Potts et al. 1990, 1997).

After a thorough literature review (Anastasopoulos 2005), a similar elastoplastic constitutive model was adopted: Mohr–Coulomb failure criterion with isotropic strain softening. The latter is introduced by reducing the mobilised friction angle φ_{mob} and the mobilised dilation angle ψ_{mob} with the increase of plastic octahedral shear strain:

$$\varphi_{\text{mob}} = \begin{cases} \varphi_p - \frac{\varphi_p - \varphi_{\text{res}}}{\gamma_f^P}\gamma_{\text{oct}}^P, & \text{for } 0 \le \gamma_{\text{oct}}^P < \gamma_f^P \\ \varphi_{\text{res}}, & \text{for } \gamma_{\text{oct}}^P \ge \gamma_f^P \end{cases} \tag{1}$$

$$\psi_{\text{mob}} = \begin{cases} \psi_p \left(1 - \frac{\gamma_{\text{oct}}^P}{\gamma_f^P}\right), & \text{for } 0 \le \gamma_{\text{oct}}^P < \gamma_f^P \\ \psi_{\text{res}}, & \text{for } \gamma_{\text{oct}}^P \ge \gamma_f^P \end{cases} \tag{2}$$

where: φ_p and φ_{res} the ultimate mobilised friction angle and its residual value; ψ_p the ultimate dilation angle; γ_f^P the plastic octahedral shear strain at the end of softening.

Model parameters are calibrated through the direct shear test. Although criticised for the non-uniformity of stresses and strains (e.g. Terzaghi and Peck 1948), due to its simplicity it remains popular in practice. Potts et al. (1987) have shown that the effect of progressive failure is only slight, allowing the interpretation of test results as quasi-simple shear. Soil response can be divided in four characteristic phases (Anastasopoulos et al. 2007a)

(a) *Quasi-elastic behaviour*: Up to a horizontal displacement δx_y the soil deforms quasi-elastically (Jewell and Roth 1987). Some non-linearity is observed, but without dilation ($-\delta y/\delta x \le 0$).
(b) *Plastic behaviour*: Beyond δx_y the soil enters the plastic region and dilates. At horizontal displacement δx_p peak conditions ($\tau/\sigma_v = \max$) are reached.
(c) *Softening behaviour*: A single horizontal shear band develops at mid-height of the specimen right after the peak (Jewell and Roth 1987; Gerolymos et al. 2007). Softening is completed at horizontal displacement $\delta x_f (\delta y/\delta x \approx 0)$.
(d) *Residual behaviour*: Shearing is accumulated along the developed shear band.

Pre-yield behaviour is modelled as linear elastic, with a secant modulus G_S linearly increasing with depth:

$$G_S = \frac{\tau_y}{\gamma_y} \tag{3}$$

where τ_y and γ_y: the shear stress and strain at first yield, directly measured from test data.

After shear band formation, it is assumed that plastic shear deformation takes place within the shear band, while the rest of the soil body remains elastic (Shibuya et al. 1997). Taking into account that scale effects play a major role in shear localisation problems (Stone and Muir Wood 1992; Muir Wood and Stone 1994; Muir Wood 2002), and given the unavoidable shortcomings of the FE method, an approximate simplified scaling method (Anastasopoulos et al. 2007a) is employed. The plastic shear strain at which softening is completed, γ_f^P, can be defined as:

$$\gamma_f^P = \frac{\delta x_p - \delta x_y}{D} + \frac{\delta x_f - \delta x_p}{d_{FE}} \tag{4}$$

where d_{FE}: the size of the finite element mesh, and D: the initial height of the soil specimen. Thus, scale effects (associated with incorrect modelling of the shear band thickness) are incorporated in the FE model in a reasonable approximate manner. Scaling is not applied to pre–shear–band parameters γ_y and γ_p.

2.2 Fault rupture–soil–foundation–structure interaction (FR-SFSI)

The model of the structure, consisting of beam elements, is placed on top of the soil model and connected through special contact (gap) elements (Fig. 1b). These elements are infinitely stiff in compression, but offer no resistance in tension. In shear their behaviour follows Coulomb's friction law. Thus, the structure is not bonded to the ground, and both uplifting and slippage can realistically occur.

The main factors influencing FR-SFSI are (see also Duncan and Lefebvre 1973; Bray 2001):

(a) The *type and continuity of the foundation system*; for example, isolated footings, mat foundation, box-type foundation, piles.
(b) The *flexural and axial rigidity of the foundation system*(thickness of mat foundation cross-section and length of tie beams, etc.)
(c) The *load of the superstructure.*
(d) The *stiffness of the superstructure* (cross section of structural members, grid spacing, presence or not of shear walls).
(e) *The soil stiffness* (G)*, strength* ($\varphi, c,$) and *kinematic parameters* (ψ).

A detailed parametric study on all five factors has been conducted in Anastasopoulos (2005). In this paper, we focus on the first three items (a, b, and c), and only in connection with the Denizevler case histories.

3 Validation of analysis methodology

3.1 Constitutive model verification

The capability of the modified Mohr–Coulomb constitutive model to reproduce soil behaviour has been validated through a series of FE simulations of the direct shear test. Figure 2 compares the results of such a simulation of Fontainebleau sand ($D_r \approx 80\%$) with experimental data (Gaudin 2002). Based on the experimental data, we use: $\varphi_p = 39°, \varphi_{\text{res}} = 30°, \psi_p = 11°, \gamma_y = 2\%$, and $\gamma_f^P \approx 13.5$ %. The comparison between simulated and laboratory curves reveals satisfactory agreement. Despite its simplicity and (perhaps) lack of generality, our constitutive model captures the predominant mode of deformation of the studied problem. Thus, we consider it to be a reasonable simplification of complex soil behaviour.

3.2 Sensitivity analysis on mesh dependency

The use of strain softening models may lead to mesh dependency (e.g. Pietruszezak and Mroz 1981). Such difficulties may be overcome by the use of higher-order constitutive models, such as non-local theory approaches (e.g. Bažant and Tsang 1984), and the Cosserat model (e.g. de Borst 1991; Gudehus and Nübel 2004). Our analysis, utilising the FE method with a strain softening constitutive law, is not immune

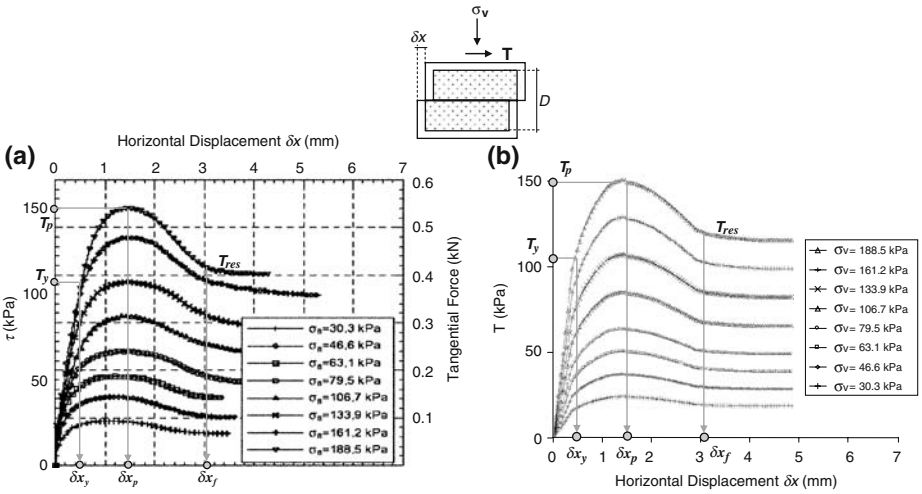

Fig. 2 Comparison between (**a**) Laboratory direct shear tests on Fontainebleau sand (Gaudin 2002), with (**b**) the results of our constitutive model. Note the definition of γ_y and γ_f.

from mesh dependency. To explore the sensitivity on mesh density, five different models with finer and coarser meshes were tested: the size of the rectangular quadrilateral elements (at the central finer region of the model) ranged from 0.25 m to 5 m. As expected, decreasing the element dimension "allowed" the deformation to be localised within a narrower band. With a coarse mesh ($d_{FE} = 5$ m) the failure zone appeared unrealistically dispersed. Condensing the mesh, the plastic zone was not only more localised, but also became smoother. There was no significant difference between the models of 0.5 m and 1.0 m element dimensions. Being advantageous from a computational point of view, we selected the latter ($d_{FE} = 1.0$ m) for the finely-meshed central region of the FE model. The adequacy of this refinement is demonstrated in detail in Anastasopoulos et al. (2007a).

3.3 Qualitative comparison with earlier published case–histories and experiments

A parametric study on fault rupture propagation through sand (in the free-field) has been presented in Anastasopoulos et al. (2007a). The consistency of the developed FE modelling methodology was first verified (Anastasopoulos 2005) through qualitative comparison with published case histories and experimental research. More specifically, the following case-histories were examined: (a) the 1954 M_s7.1 Dixie Valley Fairview Peak earthquake in Nevada (Slemmons 1957; Oakeshott 1973; Gilbert 1890), (b) the 1959 M_s7.1 Hebgen Lake earthquake in Montana (Brune and Allen 1967; Witkind et al. 1962), (c) the 1983 M_s7.3 Borah Peak earthquake in Idaho (Taylor et al. 1985; Barrientos et al. 1985; Stein and Barrientos 1985; Doser and Smith 1988). In addition, our results were compared to the experimental studies of: (i) Horsfield (1977), and (ii) Cole and Lade (1984) and Lade et al. (1984).

The results of the parametric study were concluded to be in *qualitative agreement* with both case histories and earlier experimental studies. More specifically:

- The footwall almost always remains practically intact, with most of the deformation concentrated within the hanging-wall.
- In general, the dip of a normal rupture tends to increase as it propagates towards the surface.
- "Ductile" and moderately stiff soil layers tend to spread the deformation to wider zones, decreasing the height of the fault scarp.
- When the fault dip is small ($\alpha \leq 45°$) and the soil layers stiff and brittle, secondary antithetic ruptures and gravity grabens are formed.
- In such cases ($\alpha \leq 45°$), the height of the fault scarp may exceed the imposed bedrock offset.

3.4 Class "A" Prediction of centrifuge model tests

A series of centrifuge model tests of fault rupture propagation through sand and its interaction with strip footings has been conducted in the University of Dundee, as part of the joint European research project "QUAKER". A special apparatus was developed to simulate normal and reverse faulting (Fig. 3a). Two hydraulic actuators were used to push its right part up or down, simulating reverse and normal faulting, respectively. A central guidance system (G) and three aluminium wedges (A_1–A_3) were installed to impose displacement at the desired dip angle. Perspex windows were installed at both sides to allow observation of deformation. Tests were conducted at centrifugal accelerations ranging from 50 g to 115 g. A study on the effect of stress level on fault rupture propagation is reported in El Nahas et al. (2006). Vertical and horizontal displacements at different positions within the soil were computed through image analysis using the Geo-PIV software (White et al., 2003). Additional post-processing allowed calculation of displacement profiles and strains within the deforming soil.

As for the numerical analysis, the experimental simulation of the problem was conducted in two steps. First, a series of tests were conducted to simulate fault rupture propagation in the free-field (i.e. without a footing). Fontainebleau sand (Gaudin 2002) was utilised for all of the experiments. Soil specimens were prepared by raining the sand from a specific height with controllable mass flow rate (both control the density of the sand). Before conducting four of these tests, Class "A" predictions were conducted to validate the robustness of the modelling methodology (Anastasopoulos et al. 2007a). Two normal and two reverse fault ruptures at $\alpha = 60°$ on medium-loose ($D_r \approx 60\%$) and medium-dense ($D_r \approx 80\%$) sand were selected for our simulations. The depth of the prototype soil deposit was kept constant, $H = 25$ m, while the other dimensions W, L (Fig. 3b) were varied, depending on the centrifugal acceleration level ($L = 68$ m and 75.7 m for tests conducted at 100 g and 115 g, respectively). The maximum imposed offset ranged from $h_{\max} = 1.91$ m to 3.15 m. In all cases, the FE modelling technique predicted correctly both the location of fault outcropping and the displacement profile at the ground surface (Anastasopoulos et al. 2007a).

One such comparison, in terms of vertical displacement at the surface, is reproduced in Fig. 4a. It refers to normal faulting at $\alpha = 60°$ on medium-loose sand with $D_r = 60\%$ (Test 12). Model parameters ($\varphi_p = 34°, \varphi_{\text{res}} = 30°$, $\psi_p = 6°$, $\gamma_y = 3\%$, and $\gamma_f^P = 24\%$) were calibrated following the previously discussed calibration procedure, i.e. independently of, and before, the centrifuge tests, making use of direct-shear test data on Fontainebleau sand with $D_r = 60\%$ (El Nahas et al. 2006). The analysis predicts correctly the location of fault outcropping at $d = -10$ m from the "epicenter".

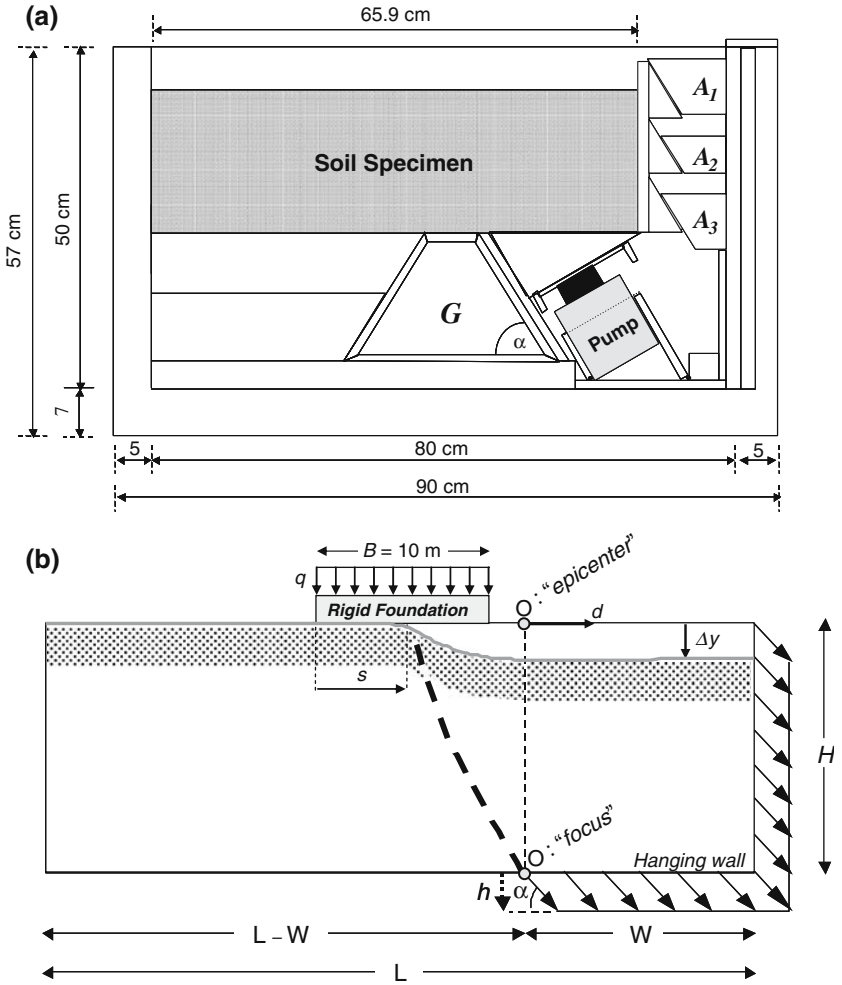

Fig. 3 (**a**) Outline of the apparatus that was installed in the Dundee University centrifuge to simulate dip slip fault rupture propagation through sand (El Nahas et at. 2006), (**b**) Model dimensions and definitions for the centrifuge model tests

The deformation seems to be slightly more localised in the experiment, but the comparison between analytical and experimental shear zone thickness remains satisfactory. For the smallest imposed dislocation, $h = 0.3$ m (experiment: $h \approx 0.24$ m), the analysis suggests a more-or-less quasi-elastic deformation at the surface, in accord with the experiment. For $h = 0.6$ m (experiment: $h \approx 0.58$ m), the deformation starts becoming localised in a relatively narrow band. Hence, the analysis is also successful in predicting the required minimum base dislocation for the fault to outcrop. For $h = 2.5$ m (experiment: $h \approx 2.47$ m) the localisation in the experiment is just a little more intense and located about 0.5 m to the left (i.e. towards the footwall) compared to our prediction. Overall, the analysis is quite satisfactory.

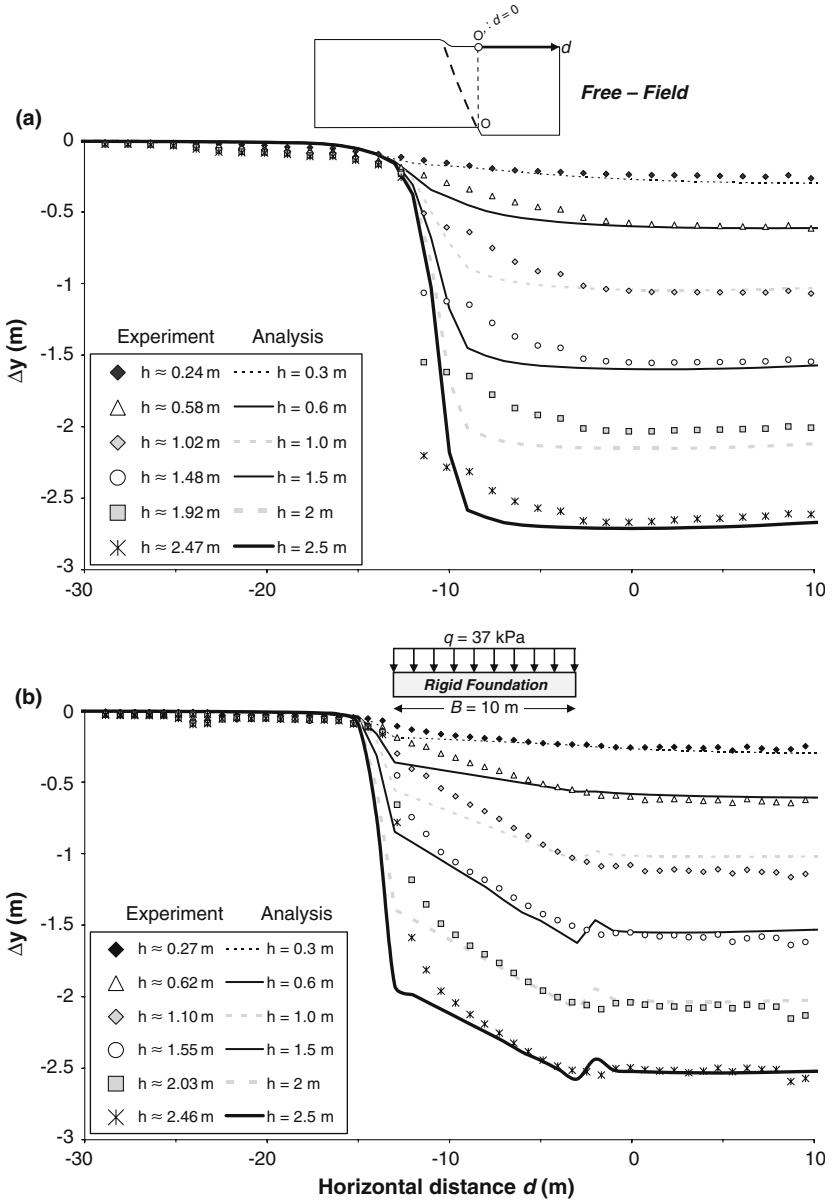

Fig. 4 Class "A" predictions of centrifuge model tests—Normal faulting at 60°, Fontainebleau sand with $Dr = 60\%$: Comparison of numerical with experimental vertical displacement of the surface for bedrock dislocation $h = 0.2$ m to 2.5 m. (**a**) Fault rupture propagation in the free field (Test 12), and (**b**) interaction with rigid footing of width $B = 10$ m and distributed load $q = 37$ kPa (Test 15). The (subsequent to analysis) centrifuge model tests produced results only at crudely approximately the pre-specified fault displacement.

At a second stage, knowing the location of fault rupture outcropping in the free-field, tests with strip footings were conducted. The aforementioned test (12) was set as the basis for fault rupture–strip footing interaction tests. A series of tests were conducted by placing strip footings at different locations relative to the fault rupture (as observed in free-field experiments). The width of the footing B was varied from 10 m to 25 m. In addition, the distributed load q was varied from 37 kPa ("light" structure) to 91 kPa ("heavy" structure) to explore its effect on fault rupture diversion and modification of the displacement profile. With the exception of one test, all footings were rigid. As for the free-field experiments, before conducting six of these tests, Class "A" predictions were conducted (Anastasopoulos et al. 2007b). In all cases examined, the analysis predicted correctly the interaction between the outcropping dislocation and the strip footing.

Figure 4b reproduces one such comparison, in terms of vertical displacement at the surface. It refers to a $B = 10$ m strip footing with distributed load $q = 37$ kPa subjected to normal faulting at $\alpha = 60°$ on medium-loose sand of $D_r = 60\%$. The footing was positioned at distances $s = 3$ m (measured from its left corner) relative to the free-field fault rupture outcrop. The analysis predicts correctly the diversion of the rupture path to the left of the footing: while in the free-field (Test 12) the rupture emerges at $d = -10$ m, due to the presence of the footing it now outcrops at $d = -13$ m (i.e. a diversion of 3 m towards the footwall). Despite this diversion, the footing does experience differential displacement, expressed as rigid body rotation. For $h = 2.5$ m (experiment: $h \approx 2.46$ m), the analysis suggests that about 0.5 m of the imposed displacement is converted to rigid body rotation, while the rest 2.0 m get localised in the form of a distinct fault scarp to the left of the footing. It is evident that the FE analysis is also successful in predicting the rotation of the footing with adequate accuracy. As it will be shown in the sequel, the extent of fault rupture diversion mainly depends on the load q.

4 Analysis of the case-histories of Denizevler

4.1 Methodology

Having validated the FE modelling methodology, we now proceed in the analysis of the Denizevler case-histories. As already discussed in the companion paper, soil conditions in the area of study do not differ significantly from one building to another. We analyse Buildings 1, 2, and 3, the Mosque, and the Basketball Court. With the exception of Building 2, which is made of cinder-block walls, all other are similar in terms of their superstructure: they are all of reinforced concrete with typical column grid in the order of 5×5 m, with strong infill brick walls. They mainly differ from one another in the number of stories and in the foundation system. The Mosque and the Basketball Court have a different structural system: the column spacing is larger, and the latter is full of shear walls along its perimeter.

Without underestimating the general importance of the details of each superstructure, we treat all of the analysed structures as "equivalent" in this respect, changing only the number of stories. This way, it is easier to develop insights on the influence of the type and stiffness of their foundation, and on the effect of the superstructure dead load on FR-SFSI. Therefore, a typical building width of 10 m and a column grid of 5×5 m is utilised. The width of the foundation B is equal to 12 m in all cases. Columns

Table 1 Properties of the five idealised structures of our FR-SFSI Analyses

	Number of stories (#)	Equivalent load (kN/m^2)	Foundation type	Rupture relative distance s[a] (m)
Building 1	4 + Basement	50	Box-type, equivalent t =1 m	10
Building 2	1	10	Separate footings, width = 2 m	2
Building 3	2 + Attic	25	Box-type, equivalent t =1 m	2
Mosque	Equivalent of 2	20	Separate footings, width = 2 m	4
Basketball court	Equivalent of 2	20	Piled foundation, pile diameter = 0.8 m	4

[a] Measured from the left corner of the building

and beams are of 50 cm square cross-section, taking account of the contribution of infill walls and slabs. Such idealisation is quite close to reality for the three buildings, and not such a bad approximation for the Mosque and the Basketball Court: their columns and shear walls may be significantly stiffer, but column spacing is also larger. Building 2 is undeniably different, but to make it a strong case and to allow for comparisons it is treated equivalently.

The five idealised structures are illustrated in Fig. 5, while their properties are summarised in Table 1. Given the multitude of structure–foundation–fault position combinations to be analysed, after reviewing the tectonics of the pull-apart basin of Gölcük, a dip angle $a = 55°$ was selected for all analyses. Although our equivalent plane-strain structural model cannot provide accurate modelling and distress estimation of the superstructure, it is regarded capable of providing comparative qualitative distress estimates. As already discussed in the companion paper, microtremor measurements of Arai et al. (2000) indicate that "sound" bedrock (with shear wave velocity $V_s = 1300$ m/sec) lies at approximately -130 m depth in the area of study. However, given the observed sharp increase of V_s from 500 m/sec to 850 m/sec at about -40 m depth, we analyse a soil deposit of depth $H = 40$ m. Based on the results of our soil investigation (Anastasopoulos and Gazetas 2007), in combination with the soil exploration of the neighboring industrial project (GEOS 2000), we analyse an idealised homogeneous soil with the following model parameters: $c = 10$ kPa, $\varphi_p = 34°, \varphi_{\text{res}} = 30°, \psi_p = 8°, \gamma_y = 2.5\%$, and $\gamma_f^P = 5\%$.

The main results of our FR-SFSI analyses are discussed in terms of deformed mesh and distribution of plastic strain, vertical displacement profile Δy, horizontal strain ε_x (positive values denote tension), and angle of distortion β along the ground surface. The latter is a characteristic measure of the deformation of ground surface; it is a useful parameter in assessing the damage potential to overlying structures. Between two points, A and B, at the ground surface β is defined as:

$$\beta = \frac{\Delta y^A - \Delta y^B}{x^A - x^B} \tag{5}$$

where Δy^A and Δy^B is the vertical displacement at points A and B, and x^A, x^B the horizontal coordinates of the two points. In all cases the results are compared with corresponding free-field results to deduce the effect of FR-SFSI. The differential settlement D_y of the foundation and the maximum bending moment $M_{\max}$ in the superstructure (beams or columns) are also reported to provide an estimate of the relative distress of each structure.

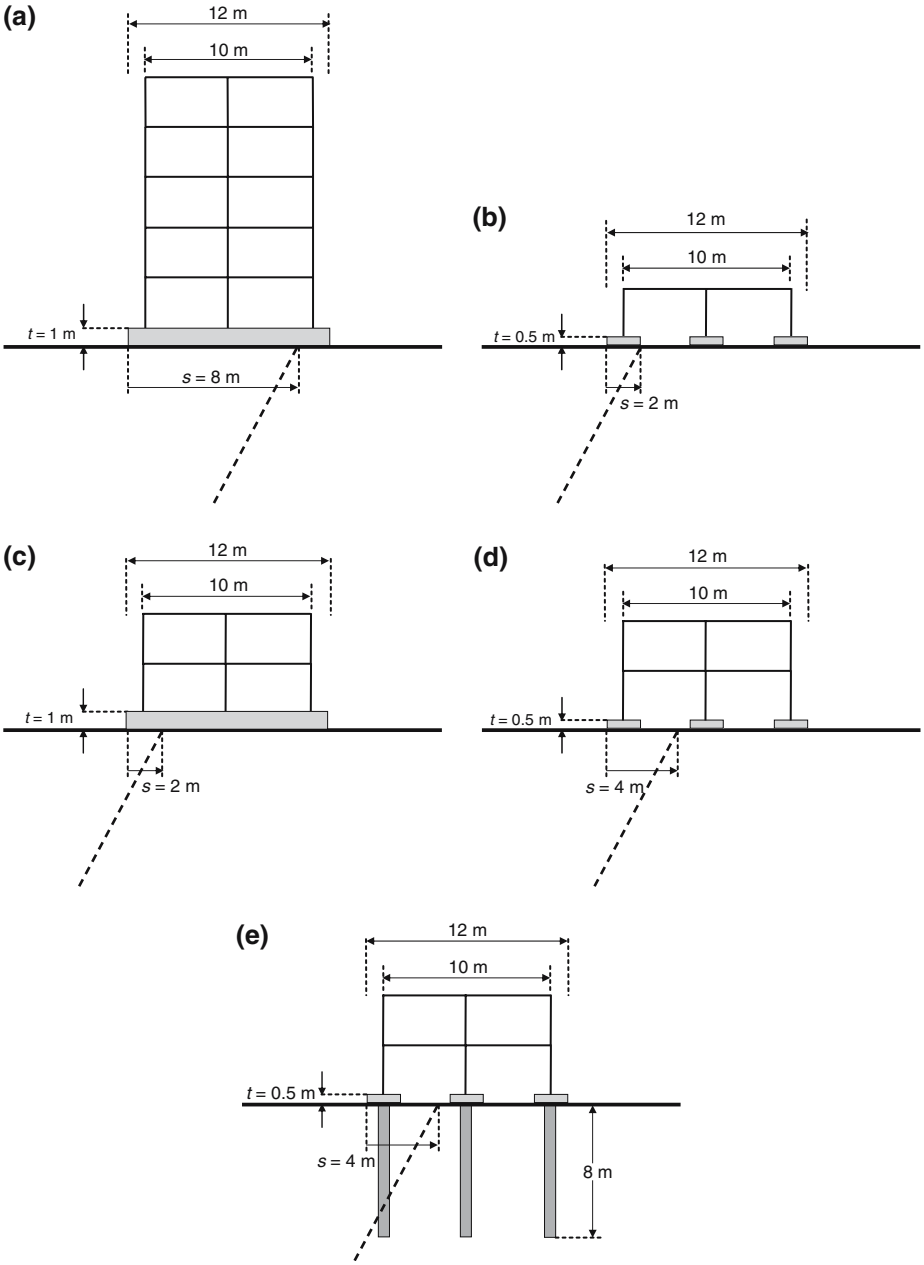

Fig. 5 Idealised structures for FR–SFSI analyses: (**a**) Building 1: 4 stories plus basement, (**b**) Building 2: 1 story, (**c**) Building 3: 2 stories, (**d**) Mosque: equivalent of 2 stories, and (**e**) Basketball Court: equivalent of 2 stories

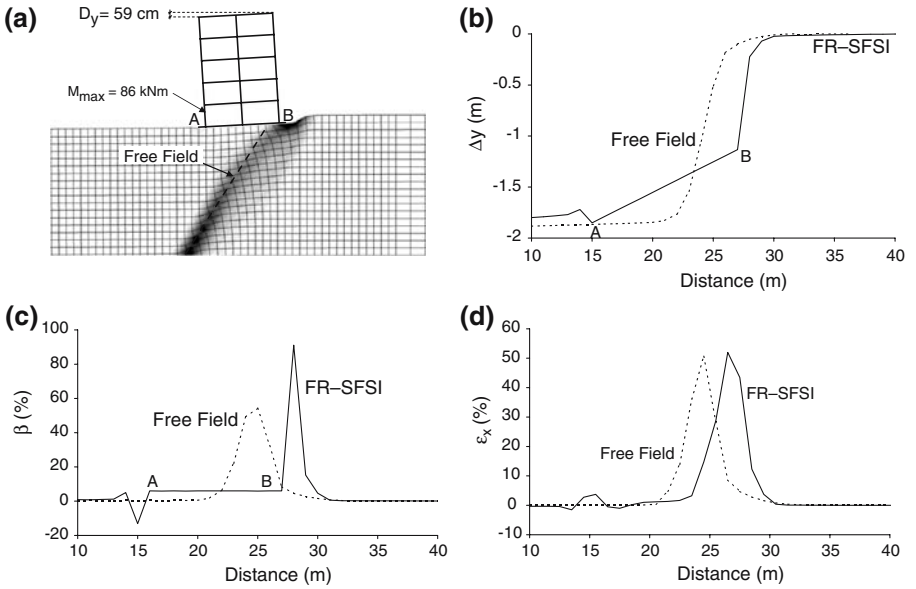

Fig. 6 FE analysis of Building 1, 4 stories + basement: (**a**) Deformed mesh and plastic strain, (**b**) Vertical displacement Δ_y at the surface, (**c**) angle of distortion β, and (**d**) horizontal strain ε_x. The results of the Fault-Rupture Soil–Foundation–Structure Interaction (FR–SFSI) analysis are compared with the Free-field.

4.2 Building 1

Figure 6 portrays the main analysis results for Building 1—representative of 5-story buildings lying on the hanging-wall with the fault rupture crossing their corner (in the free-field, i.e. in the absence of FR–SFSI). As clearly seen in Fig. 6a, the rupture path is diverted towards the footwall as it approaches the ground surface (topmost 10 m of the propagation path). In addition, the plastic strain does not remain as localised as in the free-field, but is diffused over a wider area. The building tilts towards the hanging-wall and the differential settlement D_y reaches 59 cm. Despite such significant D_y, the maximum bending moment $M_{\max}$ in the superstructure does not exceed a mere 86 kNm. This indicates that the rigid foundation not only managed to divert the rupture, but also allowed the building to rotate essentially as a rigid body, without stressing its superstructure.

The vertical displacement Δy of the ground surface (Fig. 6b), the distortion β (Fig. 6c), and the horizontal strain ε_x (Fig. 6d), all clearly indicate that the building rotates as a rigid body (tilting without significant distortion): observe region AB of constant inclination in the Δy diagram. Thus, in the β diagram, a constant slope of about 6% is maintained throughout the width of the building (AB). Compared to the free-field, the maximum distortion β is higher but is now localised just next to the building. All bears substantial similarity with what was observed in the field, where the fault scarp appeared vividly next to the building, but was subdued away from it. The horizontal ground strain ε_x is also concentrated to the right of the structure, maintaining the maximum value of the free-field.

Although the differential settlement is substantial (6% is much higher than the usually accepted maximum of 1/300), the analysis does not indicate significant distress of the building's superstructure.[1] This agrees fairly well with the observed performance: the building sustained no structural damage. However, in reality, the tilting of the building was not that large. We identify two possible explanations, in addition of course to the unavoidable modelling imperfections: (i) post-seismic consolidation of the near-the-fault edge of the building stemming from the increased contact stresses under that part of the structure, as well as from dissipation of excess pore water pressures generated from the rupturing fault, (ii) the rupture did not cross the structure perpendicularly as assumed in our analysis: it intersected only at the corner of the building (see Fig. 5 in the companion paper). Such geometry of crossing is definitely more favourable than the plane strain assumption of our analysis.

4.3 The mosque

Analysis results for the Mosque are presented in Fig. 7. Admittedly, this is not a faithful representation of the structure, but one that roughly captures the stiffness characteristics of the superstructure and its foundation. The deformed mesh reveals that the rupture follows its original (free-field) path, almost unaltered by the presence of the structure. In contrast to Building 1, where a fault scarp can be clearly identified to the right of the structure, one can now see most of the deformation taking place between the isolated footings of the Mosque, with a diffuse failure zone. The footings only barely divert the rupture from emerging directly beneath them, but not beyond the limits of the structure. The Mosque is tilting towards the hanging-wall with the differential settlement D_y reaching 1.4 m. Unlike the previous case, D_y is not "absorbed" by the rigidity of the foundation. The Mosque not only rotates as a rigid body, but is also substantially distressed (tilting with significant distortion). The maximum bending moment $M_{\max}$ in its structural elements reaches 945 kNm. Such stressing would certainly cause collapse, given the dimensions and reinforcement of its structural members. The vertical displacement Δy, the distortion β, and the horizontal strain ε_x, all clearly indicate that very little interaction takes place between the rupturing plane and the structure. In other words, FR-SFSI is hardly affecting the emergence of the rupture on the ground surface. Compared to the free-field, the maximum distortion β remains almost unaltered, and occurs at about the same location. The horizontal tensile strain is spread over a wider area, but its peak is almost half of the free-field. In conclusion, the FR-SFSI analysis agrees quite well with the actual performance of the Mosque.

4.4 Building 2

Figure 8 summarises the results for Building 2 (on isolated strip footings). The model is an approximation of the actual cinder-block wall superstructure. The rupture is only locally diverted towards the hanging-wall to avoid the far-left footing of the building. The dislocation follows the same propagation path as in the free-field, with the exception of the top 4 m before outcropping. The building tilts towards the hanging-wall, with the differential settlement D_y not exceeding 33 cm. Despite the smaller D_y,

[1] For some interesting case histories of building titling the reader is referred to the recent article by Charles and Skinner (2004), where it is shown that tilting by 5.5% of a building on stiff raft caused only slight wall cracking.

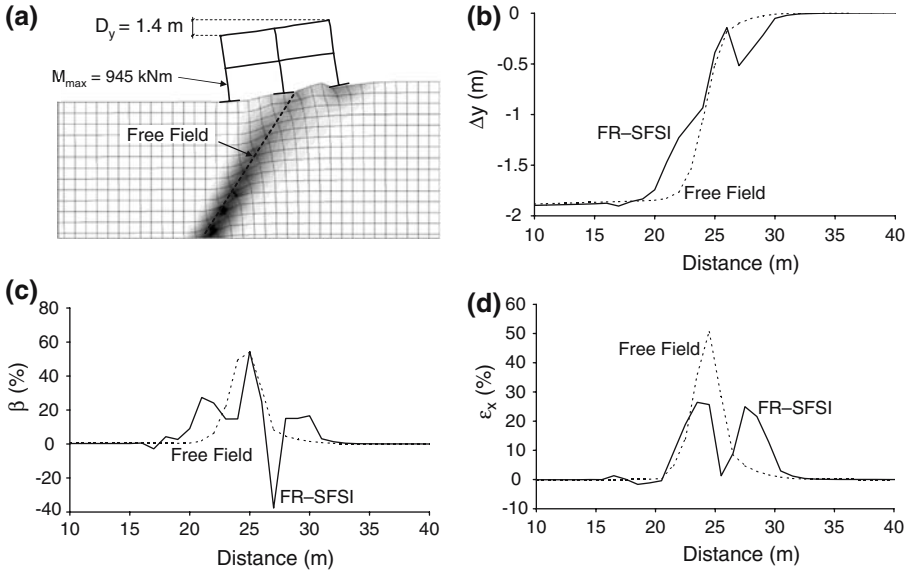

Fig. 7 FE analysis of the Mosque, equivalent of 2 stories: (**a**) Deformed mesh and plastic strain, (**b**) Vertical displacement Δ_y at the surface, (**c**) angle of distortion β, and (**d**) horizontal strain ε_x. The results of the Fault-Rupture Soil–Foundation–Structure Interaction (FR–SFSI) analysis are compared with the Free-field.

compared to the previous cases, $M_{\max}$ reaches 469 kNm. Evidently, such distress could not be accommodated by the cinder-block walls of this structure. Observe that a part of the edge footing is detached from the ground. The vertical displacement Δy, the distortion β, and the horizontal strain ε_x, all reveal that FR-SFSI does not affect either the dislocation path, or the surface displacement profile. Compared to the free-field, β is only slightly higher and similarly localised, while the maximum ε_x is only marginally lower. In conclusion, it can safely be argued that the FE analysis agrees quite well with the observed performance of Building 2, despite the crude approximation of the superstructure. In reality, the superstructure of this building was far more brittle than assumed in our analysis. In any case, the results indicate partial collapse.

4.5 Building 3

Figure 9 depicts the results for Building 3. Until reaching a depth of about 12 m, the rupture follows the same propagation path as in the free-field. Then, it is diverted to the left of the building, towards the hanging-wall. The plastic strain seems to be quite localised and a distinct fault scarp is numerically predicted. The building tilts slightly towards the hanging-wall, and the differential settlement D_y does not exceed 23 cm. Despite this considerable D_y, $M_{\max}$ reaches merely 121 kNm. Again, as in the case of Building 1, the rigid and continuous box-type foundation not only succeeds in diverting the dislocation (even if barely), but it also "converts" the differential displacement to rigid body rotation. The vertical displacement Δy, the distortion β, and the horizontal strain ε_x, are all in accord with the aforementioned response. Regarding Δy, the soil–foundation contact surface AB plots a straight line. In the β profile AB indicates a constant slope of about 2%, maintained across the width of the building

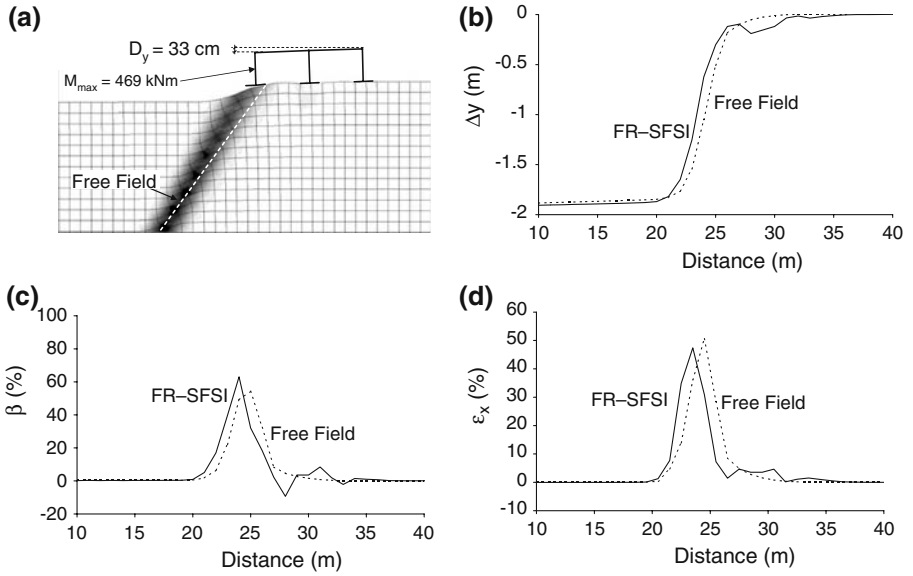

Fig. 8 FE analysis of Building 2, 1 story: (**a**) Deformed mesh and plastic strain, (**b**) Vertical displacement Δ_y at the surface, (**c**) angle of distortion β, and (**d**) horizontal strain ε_x. The results of the Fault-Rupture Soil–Foundation–Structure Interaction (FR– SFSI) analysis are compared with the Free-field.

(tilting without distortion). Compared to the free-field, the maximum distortion β is only slightly higher and just a little more localised, but it appears just next to the building. The horizontal strain ε_x is also localised to the left of the building. Although D_y is an appreciable 2%, no sign of distress is predicted for the building. One must realise that despite the commonly accepted 1/300 rule of desired maximum tilt, a 2% tilting is not easily observable and as seen in the article of Charles and Skinner (2004) would not cause any structural distress in buildings on stiff rafts. Of interest are some additional examples from the Kocaeli (Turkey) earthquake. For instance, there were many buildings in Adapazari with post-seismic tilting of about 3°(≈5%), or more, that exhibited absolutely no structural damage (Gazetas et al. 2003). This is always the case when the foundation is continuous and rigid enough to "convert" the differential settlement to rigid-body rotation. As a conclusion, the FR-SFSI analysis agrees well (at least qualitatively) with the observed performance of Building 3.

4.6 Basketball court

Our FR-SFSI analysis results for a small part of the Basketball Court are summarised in Fig. 10. Note that the dislocation follows its free-field propagation path up to the vicinity of the corner pile, at a depth of about 10 m. It is then strongly diverted towards the hanging-wall (to the left of the building). Plastic strain is localised in a very narrow band and a distinct fault scarp develops right next to the pile (Fig. 10a). The building tilts slightly towards the hanging-wall with the differential settlement D_y not exceeding 7 cm, while at the same time the left pile cap loses contact with the ground—in accord with our field observations (seen clearly in Fig. 10 of the companion paper). Surprisingly, despite the relatively minor D_y, the distress of the superstructure is quite

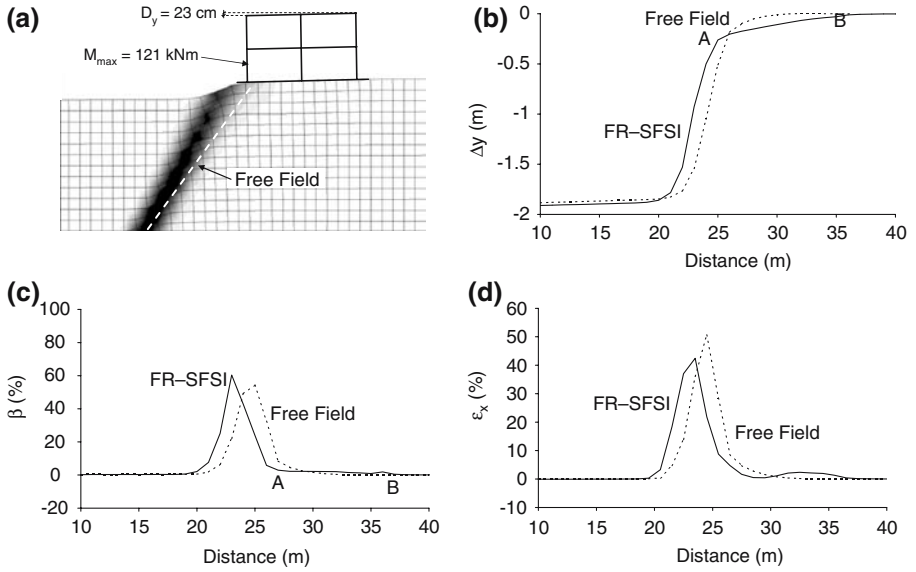

Fig. 9 FE analysis of Building 3, 2 stories plus attic: (**a**) Deformed mesh and plastic strain, (**b**) Vertical displacement Δ_y at the surface, (**c**) angle of distortion β, and (**d**) horizontal strain ε_x. The results of the Fault-Rupture Soil–Foundation–Structure Interaction (FR–SFSI) analysis are compared with the Free-field.

substantial: $M_{\max}$ reaches almost 400 kNm. Although the piles divert the dislocation, some differential settlement and, especially, differential extension takes place between the columns of the structure. This small but non-negligible deformation is imposed on the superstructure by the piles. The latter are being pulled down and out (even if slightly) by the downward moving hanging-wall, thereby forcing the superstructure to follow. In contrast to the *continuous and rigid* box-type foundation of Buildings 1 and 3, the *discontinuous* piled foundation does not allow the superstructure to rotate as a rigid body without being distorted. The vertical displacement Δy, the distortion β, and the horizontal strain ε_x, all agree with the aforementioned response. Notice the significant increase of β and its localisation right to the left of the corner pile.

In conclusion, our analysis predicts significant distress at the corner of the Basketball Court, agreeing well with its actual performance. However, the limitations of our model for the piled foundation must be clearly spelled out. The plane strain assumption implies that our "piles" are in (the computational) reality continuous "walls" (diaphragm type). Such walls are subjected to higher normal actions (per unit length) from the downward and outward moving soil than individual piles. This is because: (i) soil can "flow" around the piles, but not around the plane "wall"; (ii) the frictional capacity of the pile–soil interface is not unlimited, as implicitly assumed in our "bonded" model, thus making the downward "flow" of the soil even easier; and (iii) in reality the corner piles failed in tension, thus reducing their pulling-down of the superstructure (allowing it not to follow ground deformation completely). Nevertheless, in a qualitative sense the results of our (admittedly imperfect) analysis reveal the trends that were observed in the field.

To further investigate the role of the piled foundation, we analyse the same building but with a *continuous and rigid* box-type foundation instead of piles. As depicted in

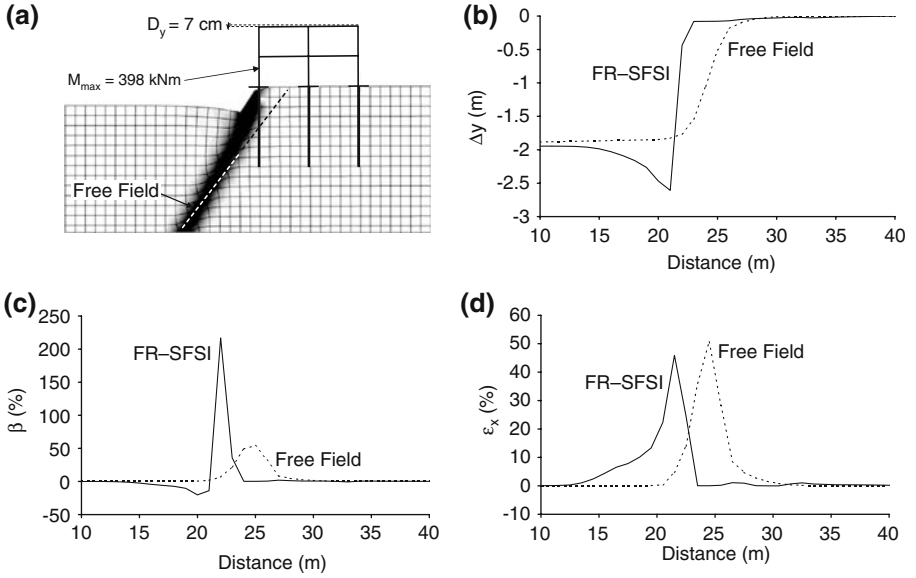

Fig. 10 FE analysis of the Basketball Court, equivalent of 2 stories: (**a**) Deformed mesh and plastic strain, (**b**) Vertical displacement Δ_y at the surface, (**c**) angle of distortion β, and (**d**) horizontal strain ε_x. The results of the Fault-Rupture Soil– Foundation–Structure Interaction (FR–SFSI) analysis are compared with the Free-field.

Fig. 11, the dislocation is again diverted towards the hanging-wall, but is more diffuse and creates a smoother surface settlement profile. The rupture follows its free-field propagation path from the base rock up to a depth of about 12 m. It then diverts towards the hanging-wall (to the left of the building). The distortion angle β is much less localised compared to the piled alternative, maintaining essentially the same value as in the free-field. The building now tilts more with the differential settlement D_y reaching 57 cm. Nevertheless, as expected, the superstructure is not distressed: $M_{\max} = 121$ kNm, only. The Basketball Court could most likely have behaved better had it been founded on a continuous rigid box-type or raft foundation, rather than on piles.

5 The effect of the weight of the superstructure

So far, only simplified models of the five structures observed in Denizevler were studied. Our FE analysis results were shown to be consistent with reality. The type, continuity, and rigidity of the foundation system (isolated footings or piles versus rigid raft or box-type foundations) were found to play a decisive role.

On the other hand, increasing the load of the superstructure increases the stresses $\Delta\sigma$ under the foundation. As repeatedly noted, the dislocation starts diverting at a certain depth below the structure which could be associated with the region affected by $\Delta\sigma$. In all cases the rupture remains unaffected at higher depths, where $\Delta\sigma$ is negligible compared to geostatic stresses. In case of buildings on raft or box-type foundations, the diversion starts at about 12 m depth, which is equal to the width B

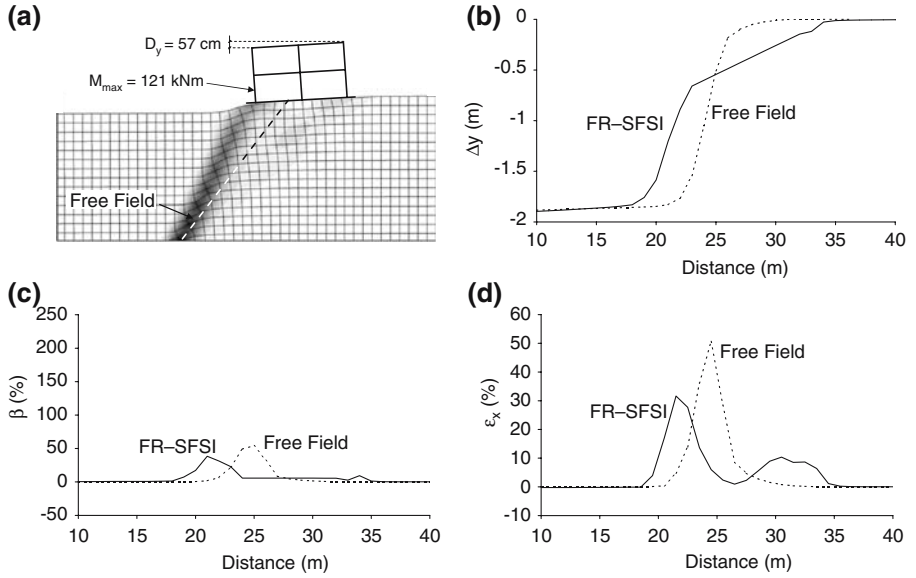

Fig. 11 FE analysis of the Basketball Court, after hypothetically replacing the piles with a stiff raft foundation $t = 1.0\,\text{m}$: (**a**) Deformed mesh and plastic strain, (**b**) Vertical displacement Δ_y at the surface, (**c**) angle of distortion β, and (**d**) horizontal strain ε_x. The results of the Fault-Rupture Soil–Foundation–Structure Interaction (FR–SFSI) analysis are compared with the Free-field.

of the generalised footing. Similarly, for buildings founded on separate footings the diversion (if any) takes place at depths similar to the width of their isolated footings ($\approx 2\,\text{m}$).

To investigate the implied effect of the superstructure induced stresses on FR-SFSI, a parametric study is performed and its results are depicted in Fig. 12. Keeping all other parameters constant, three building frames were analysed with the only difference being the load q of the superstructure, i.e. the number of stories:

- a 2-story building: $q = 20\,\text{kN/m}^2$
- a 4-story building: $q = 40\,\text{kN/m}^2$
- a 8-story building: $q = 80\,\text{kN/m}^2$

The foundation is invariably of a box-type, of equivalent slab thickness $t = 1\,\text{m}$. The buildings are positioned at distances $s = 2, 4, 8$, and $10\,\text{m}$ (measured from their left corner) relative to the free-field fault rupture outcrop.

In all cases, increasing the load tends to improve the performance of the superstructure. As shown in Fig. 12a, for $s = 2\,\text{m}$, while the 2-story building ($q = 20\,\text{kN/m}^2$) diverts the rupture only slightly (1 m) to the left, the 4-story ($q = 40\,\text{kN/m}^2$) building diverts the dislocation by more than 2 m. On the other hand, as seen in the values of β, there is no significant difference on the tilting of the two structures. While the 4-story structure is not loosing contact with the bearing soil, the lighter 2-story model separates from the ground at point a and behaves as a cantilever for a length of about 2 m (left side). The situation is different with the 8-story building (Fig. 13): the increase of $\Delta\sigma$ initially leads to diversion of the rupture to the right of the building. Further increase of the imposed bedrock offset h to 2m leads to the development of a second

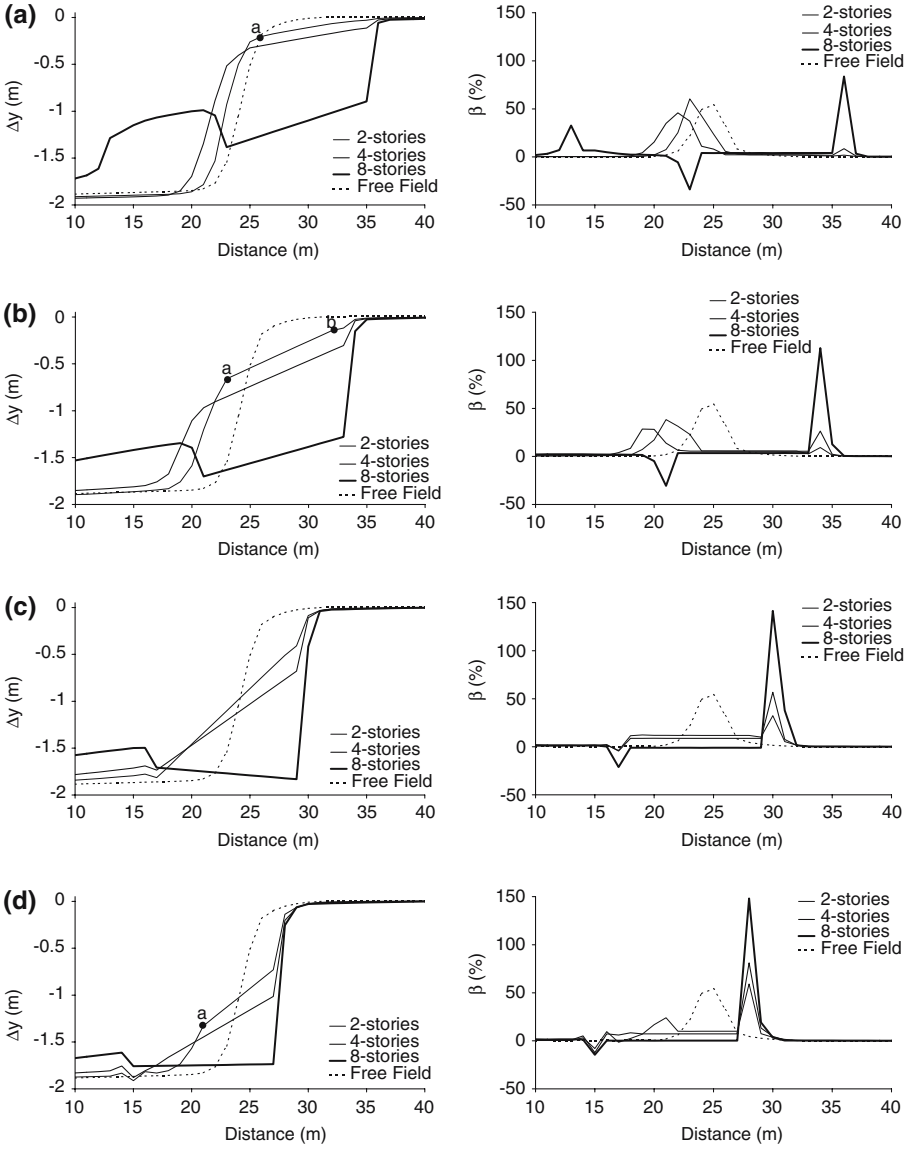

Fig. 12 Summary of vertical displacement Δ_y and distortion angle β: (**a**) $s = 2\,\text{m}$, (**b**) $s = 4\,\text{m}$, (**c**) $s = 8\,\text{m}$, and (**d**) $s = 10\,\text{m}$ (s: distance of the left corner of the building from the point where the rupture would emerge at the surface in the free-field)

rupture which outcrops at about 10 m left of the building, and yet a third rupture emerging just next to the left corner of the structure.

Figure 12b depicts the results for $s = 4\,\text{m}$. Again, the 4-story building forces the rupture to divert by more than about 5 m towards the hanging-wall, while the 2-story achieves only a 1.5 m diversion. Again, there is no significant difference in tilting. But the 4-story structure remains in contact with the overlying soil, while the 2-story

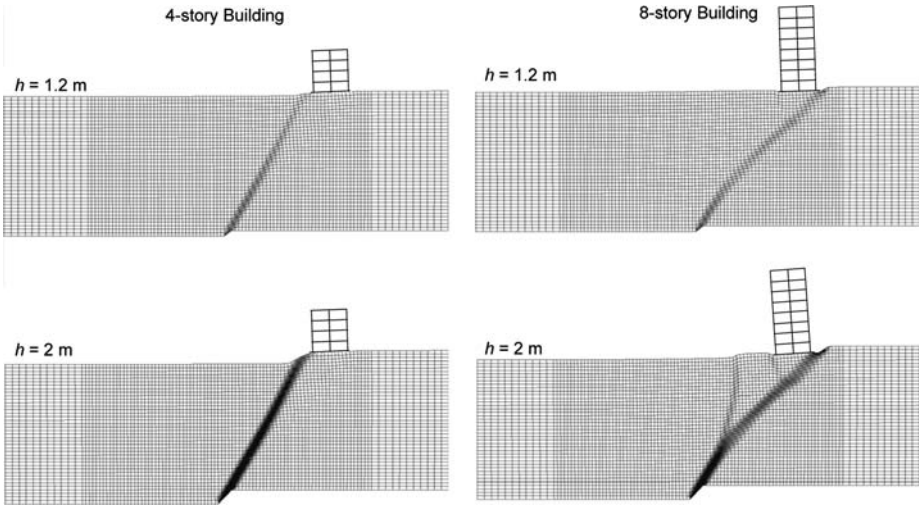

Fig. 13 4-story building vs 8-story building, rupture would outcrop at $s = 2$ m to the right of the left edge in the free-field: comparison of deformed mesh and plastic strain for $h = 1.2$ m and 2 m

structure separates from the ground both at its left (for about 2.5 m) as well as at its right (for about 3 m) (the contact is retained along *ab* only). As in the previous case, the 8-story structure diverts the rupture by more than 8 m to the right of the building, with the tilting becoming significantly decreased.

By moving the relative position of the rupture to the right side of the examined structures the situation becomes a little different. As shown in Fig. 12c, for $s = 8$ m, while the 2-story building tends to divert the dislocation towards the hanging-wall, the heavier 4-story structure ($q = 40\,\text{kN/m}^2$) manifests a completely different response: the rupture is now diverted towards the footwall. In the first case, the diversion is about 5 m to the left, while in the second case it reaches 7 m to the right. As seen in β, the tilting of the two structures is also different, with the heavier building tilting less (8.5% instead of 12%). The situation is similar for the 8-story building with the exception that the tilting of the structure would diminish and reverse.

Finally, Fig. 12d illustrates the results for $s = 10$ m. Now, both buildings divert the rupture towards the footwall, with the heavier one achieving sharper deformation localisation. As in the previous case, the tilting of the two structures is different with the heavier tilting less (7% instead of 10%). The 4-story structure remains in contact with the underlying soil throughout its foundation length, while the 2-story building debonds at its left after point *a* (separation length ≈ 3 m). Again, as depicted in Fig. 14 the 8-story building diverts the rupture to the right (towards the footwall), remaining practically vertical without any tilting taking place.

6 Conclusions

The main conclusions of our study are as follows:

1. The developed FE modelling technique, assuming plane strain conditions, reproduces reality in all of the examined cases at least qualitatively. Some differences

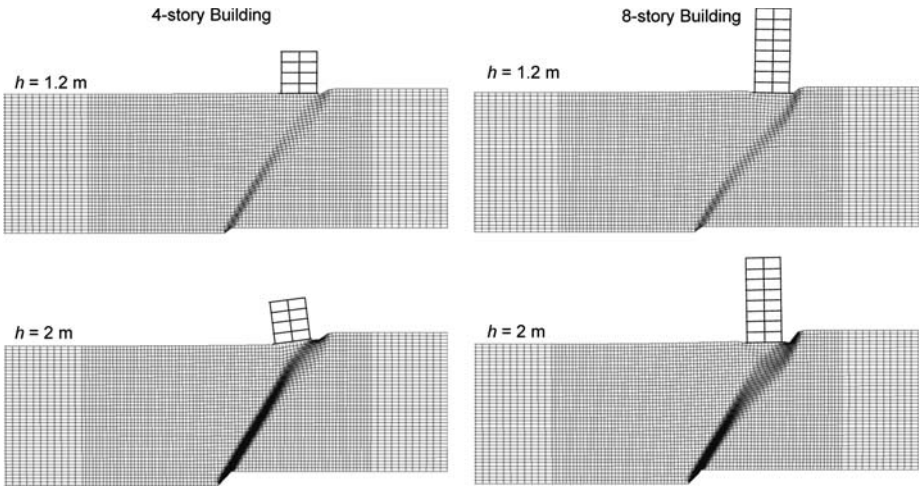

Fig. 14 4-story building vs 8-story building, rupture would outcrop at $s = 10$ m to the right of the left edge in the free-field: comparison of deformed mesh and plastic strain for $h = 1.2$ m and 2 m

between analysis and reality (for Building 1, for example) could be attributed to the actual geometry of the building–rupture intersection, which is modeled only crudely. Validation through Class "A" predictions of centrifuge model tests strengthens the validity of our conclusions.

2. The type, continuity, and rigidity of the foundation system have a profound effect on the response of a structure over an outcropping fault rupture. Structures lying on *continuous and rigid* mat or box-type foundations perform much better than the ones on *discontinuous* isolated footings or piles. The real-scale natural experiment of Denizevler provides valuable evidence, which is verified by the FR-SFSI analyses presented herein.
3. Buildings founded on *continuous and rigid* box-type foundations, may force the outcropping rupture to divert. Even if the diversion is partial, the rigidity of such foundations "spreads" the deformation and allows the structure to rotate as a rigid body, without experiencing significant distortion and distress. The structure may locally separate from the supporting soil, and may thus be relieved from the imposed displacements. Apparently, reinforced-concrete buildings can perform as cantilevers or simply supported beams to bridge locally generated "small" gaps, provided that they are founded on *continuous and rigid* foundations. Buildings 1 and 3 are the real examples of this encouraging performance, which is verified through our FR-SFSI study.
4. Buildings on *discontinuous* isolated footings may only *very locally* divert the rupture (to avoid emerging right beneath a footing). The rupture outcrops within the limits of the structure, imposing substantial distortion and detrimental structural distress. Building 2 and the Mosque are the actual proof of the inferior performance of separate footing founded buildings compared to structures on mat or box-type foundations. Tie beams can ameliorate the performance of buildings founded on isolated footings, by rigidifying their base.
5. Buildings lying on *discontinuous* piles (i.e. without a continuous pile cap) are found to perform much worse than the ones on continuous and rigid (mat or box-type)

foundation systems. Although a piled foundation could divert the dislocation, it tends to force the superstructure to follow the imposed deformation: the structure is not allowed to be relieved by loosing contact with the deformed soil surface, as in the case of mat (or box-type) foundations. This causes significant distortion and distress of the superstructure, as witnessed by the relatively poor performance of the Basketball Court. In that particular case, had the piles not failed in tension the distress of the building could have been even worse. The capacity design, allowing the superstructure to yield and requiring the piles to remain elastic, should be revised in this respect. Possibly, the piles should be designed to fail before the superstructure, in order to armor it form the imposed differential displacements.

6. The effect of the superstructure's dead load q is equally important. The increase of q augments the stress change beneath the foundation, which consequently increases the diversion of the dislocation. The dislocation finds it easier to propagate by rupturing the soil with less strength. Therefore, since the soil underneath the building is of higher strength, due to the additional confinement (stress increase) provided by the load q, it is profitable for the rupture to bend and avoid the higher strength area right beneath the structure. The presence of high water table, by decreasing the effective stress, amplifies the effect of q: for the same load the stress change will be proportionately higher. In cohesive soils or rocky materials, where the strength is more-or-less independent of confinement, we would not expect the rupture to divert significantly.
7. Structures in the vicinity of active faults can be designed to withstand tectonic dislocations. This paper provides a first step for the development of an analysis methodology towards this direction. Simple and relatively poor residential structures are proven to perform quite well (reality agrees with our centrifuge-validated analysis). The "secret" of their success is proven to lie on the continuity, stiffness, and rigidity of their box-type foundation. Founding buildings on separate footings should be avoided in such cases, while piled foundations are considered to be problematic.

Acknowledgements This work formed part of the EU research project "QUAKER" which is funded through the EU Fifth Framework Programme: Environment, Energy, and Sustainable Development, Research and Technological Development Activity of Generic Nature: the Fight against Natural and Technological Hazards, under contract number: EVG1-CT-2002-00064. We wish to express our sincerest gratitude to Professor M.C.R. Davies and Dr. M.F. Bransby for designing and conducting centrifuge model tests of excellent quality. The validity of the derived conclusions largely depends on their experimental work. *Partial support by* OASP (Organization for Antiseismic Protection of Greece) is also acknowledged. We thank Mr. I. N. Sigalas for his valuable support and Professor S. Pavlides for providing the geological cross-sections and all the relevant geologic information.

References

Anastasopoulos I (2005) Fault rupture-soil-foundation-structure interaction, Ph.D. Dissertation, School of Civil Engineering, National Technical University, Athens, pp. 570

Anastasopoulos I, Gazetas G (2007) Foundation-structure systems over a rupturing normal fault: Part I. Observations after the Kocaeli 1999 earthquake, Bulletin of Earthquake Engineering (companion paper) DOI 10.1007/s10518-007-9029-2

Anastasopoulos I, Gazetas G, Bransby MF, Davies MCR, El Nahas A (2007a) Fault rupture propagation through sand: finite element analysis and validation through centrifuge experiments. J Geotech Geoenviron ASCE (in print)

Anastasopoulos I, Gazetas G, Bransby MF, Davies MCR, El Nahas A (2007b) Normal fault rupture interaction with strip foundations. J Geotech Geoenviron ASCE (Submitted)
Arai H, Hibino H, Okuma Y, Matsuoka M, Kubo T, and Yamazaki F (2000) Estimation of ground motion characteristics and damage distribution in golcuk, turkey, based on microtremor measurements, In: Proc 6th International Conference on Seismic Zonation.
Barrientos SE, Ward SN, Gonzalez-Ruiz JR, Stein RS (1985) Inversion for moment as a function of depth from geodetic observations and long period body waves of the 1983 Borah Peak, Idaho earthquake. U.S. Geological Survey Open-file Report 85–290, pp 485–518
Bažant ZP, Tsang TP (1984) Non local finite element analysis of strain softening solids. J Eng Mech ASCE 110(12):1441–1450
Bray JD (1990) The effects of tectonic movements on stresses and deformations in earth embankments. Ph.D Dissertation, University of California, Berkeley
Bray JD (2001) Developing mitigation measures for the hazards associated with earthquake surface fault rupture. Workshop on Seismic Fault-Induced Failures – Possible Remedies for Damage to Urban Facilities, University of Tokyo Press, pp 55–79
Bray JD, Seed RB, Seed HB (1993) 1 g small-scale modelling of saturated cohesive soils. Testing J American Society for Testing and Materials 16(1):46–53
Bray JD, Seed RB, Cluff LS, Seed HB (1994) Earthquake fault rupture propagation through soil. J Geotech Eng, ASCE 120(3):543–561
Bray JD, Seed RB, Seed HB (1994b) Analysis of earthquake fault rupture propagation through cohesive soil. J Geotech Eng ASCE 120(3):562–580
Brune JN, Allen CR (1967) A low-stress-drop, low magnitude earthquake with surface faulting. The Imperial, California, Earthquake of March 4, 1966. Bull Seismol Soc Am 57:501–514
Cole DA Jr, Lade PV (1984) Influence zones in alluvium over dip-slip faults. J Geotech Eng ASCE 110(5):599–615
Charles JA, Skinner HD (2004) Settlement and tilt of low-rise buildings. Geotech Eng 157(GE2):65–75
de Borst R (1991) Simulation of strain localization: a reappraisal of the Cosserat continuum. Engng Comput 8:317–332
Doser DI, Smith RB (1988) Source parameters of the 28 October 1983 Borah Peak, Idaho, earthquake from body wave analysis. Bull Seismol Soc Am 75:1041–1051
Duncan JM, Lefebvre G (1973) Earth pressures on structures due to fault movement. J Soil Mech Found Div 1153–1163
El Nahas A, Bransby MF, Davies MCR (2006) Centrifuge modelling of the interaction between normal fault rupture and rigid, strong raft foundations. In: Proc. International Conference on Physical Modelling in Geotechnics, Hong Kong, August, pp 337–342
Erickson SG, Staryer LM, Suppe J (2001) Initiation and reactivation of faults during movement over a thrust-fault ramp: numerical mechanical models. J Struct Geol 23:11–23
Gaudin C (2002) Experimental and theoretical study of the behaviour of supporting walls: validation of design methods. Ph d dissertation, Laboratoire Central des Ponts et Chaussées, Nantes, France
Gazetas G, Apostolou M, Anastasopoulos I (2003) Seismic uplifting of foundations on soft soil, with examples from Adapazari (Izmit 1999, Earthquake). BGA International Conference on Foundations: Innovations, Observations, Design and Practice, University of Dundee, Scotland, September 2–5, pp 37–50
Gerolymos N, Vardoulakis I, Gazetas G (2007) A thermo-poro-viscoplastic shear band model for seismic triggering and evolution of catastrophic landslides. Soils Found 47(1) (in press)
GEOS (2000) Geotechnical evaluation report for the Gölcük Kücük Industrial Project, August 2000 (in Turkish)
Gilbert GK (1890) Lake Boneville US, Geological Survey Monthly 1, 1890
Gudehus G, Nübel K (2004) Evolution of shear bands in sand. Géotechnique 54(3):187
Horsfield WT (1977) An experimental approach to basement-controlled faulting. Geologie En Mijnboyw 56(4):363–370
Jewell RA, Roth CP (1987) Direct shear tests on reinforced sand. Géotechnique 37(1):53–68
Lade PV, Cole DA Jr, Cummings D (1984) Multiple failure surfaces over dip-slip faults. J Geotech Eng, ASCE 110(5):616–627
Lambe TW (1973) Predictions in soil engineering. Géotechnique 23(2):149–202
Loukidis D (1999) Active fault propagation through soil. Diploma Thesis, National Technical University, Athens
Muir Wood D (2002) Some observations of volumetric instabilities in soils. Int J Solids Struct 39:3429–3449

Muir Wood D, Stone KJL (1994) Some observations of zones of localisation in model tests on dry sand. In: Chambon R, Desrues J, Vardoulakis I (eds) Localisation and Bifurcation Theory for Soils and Rocks, A.A. Balkema, Rotterdam, pp 155–164
Oakeshott GB (1973) Patterns of ground ruptures in fault zones coincident with earthquakes: some case histories, the Association of Engineering Geologists. Reprinted from geology, Seismicity, and Environmental Impact, Special Publication, October, pp 287–312
Pietruszezak ST, Mroz Z (1981) Finite element analysis of deformation of strain softening materials. Int J Numer Meth Eng 17:327–334
Potts DM, Dounias GT, Vaughan PRV (1987) Finite element analysis of the direct shear box test. Géotechnique 37(1):11–23
Potts DM, Dounias GT, Vaughan PR (1990) Finite element analysis of progressive failure of Carsington Embankment. Géotechnique, 40(1):79–101
Potts DM, Kovacevic N, Vaughan PR (1997) Delayed collapse of cut slopes in stiff clay. Géotechnique 47(5):953
Roth WH, Scott RF, Austin I (1981) Centrifuge modelling of fault propagation through alluvial soils. Geophys Res Lett 8(6):561–564
Roth WH, Sweet J, Goodman RE (1982) Numerical and physical modelling of flexural Slip phenomena and potential for fault movement. Rock Mech (Suppl 12):27–46
Scott RF, Schoustra JJ (1974) Nuclear power plant siting on deep alluvium. Journal of the Geotechnical Engineering Division ASCE 100(GT4):449–459
Shibuya S, Mitachi T, Tamate S (1997) Interpretation of direct shear box testing of sands as quasi-simple shear. Géotechnique 47(4):769–790
Slemmons DB (1957) Geological effects of the Dixie Valley-Fairview Peak, Nevada, Earthquakes of December 16, 1954. Bull Seismol Soc Am 47(4):353–375
Stein RS, Barrientos SE (1985) The Borah Peak Idaho earthquake-geodetic evidence for deep rupture on a planar fault. U.S., Geological Survey, Open-File Report 85–250, pp 181–234
Stone KJL, Muir Wood D (1992) Effects of dilatancy and particle size observed in model tests on sand. Soils Found 32(4):43–57
Taylor CL, Cline KM, Page WD, Schwartz DP (1985) The Borah Peak, Idaho earthquake of October 28, 1983 - surface faulting and other phenomena. Earthquake Spectra 2(1):23–49
Terzaghi K, Peck RB (1948) Soil mechanics in engineering practice. John Wiley, New York
White DJ, Take WA, Bolton MD (2003) Soil deformation measurement using particle image velocimetry (PIV) and photogrammetry. Géotechnique 53(7):619–631
Witkind IJ, Myers WB, Hadley JB, Hamilton W, Fraser GD (1962) Geologic features of the earthquake at Hebgen Lake, Montana, August 17, 1959. Bull Seismol Soc Am 52(2):163–180